Efficient Pt(ii) emitters assembled from neutral bipyridine and dianionic bipyrazolate: designs, photophysical characterization and the fabrication of non-doped OLEDs

Efficient Pt(II) Emitters Assembled from Neutral Bipyridine and Dianionic Bipyrazolate: Designs, Photophysical Characterizations and Fabrication of Non-doped OLEDs

Che-Wei Hsu,[a,‡] Yongbiao Zhao,[b,‡] Hsiu-Hsuan Yeh,[a] Chin-Wei Lu,[a] Cong Fan,[a] Yue Hu,[c] Neil Robertson,[c,*] Gene-Hsiang Lee,[d] Xiao Wei Sun,[b,*] and Yun Chi[a,*]

[a] C.-W. Hsu, Dr. H.-H. Yeh, Dr. C.-W. Lu, Dr. C. Fan, Prof. Y. Chi

Department of Chemistry, National Tsing Hua University, Hsinchu 30013, Taiwan;

E-mail: ychi@mx.nthu.edu.tw

[b] Dr. Y. Zhao, Prof. X. W. Sun

Center of Excellence for Semiconductor Lighting and Displays, School of Electrical and Electronic Engineering, Nanyang Technological University, 50 Nanyang Avenue, Singapore 639798, Singapore; E-mail: exwsun@ntu.edu.sg

[c] Y. Hu, Prof. N. Robertson

School of Chemistry, The University of Edinburgh, The King's Buildings, David Brewster Road, Edinburgh EH9 3FJ, United Kingdom; E-mail: Neil.Robertson@ed.ac.uk

[d] Dr. G.-H. Lee

Instrumentation Center, National Taiwan University, Taipei 10617, Taiwan

Abstract

A potential dianionic chelate, 5,5'-bis(trifluoromethyl)-2H,2'H-3,3'-bipyrazole (bipzH$_2$) and 5,5'-(1-methylethylidene)-bis(3-trifluoromethyl-1H-pyrazole) (mepzH$_2$), were synthesized from Claisen condensation employing ethyl trifluoroacetate with 2,3-butanedione and with 3,3-dimethyl-2,4-pentanedione, followed by hydrazine cyclization. These chelates were then utilized in preparation of four emissive Pt(II) metal complexes [Pt(tbbpy)(bipz)] (**1**), [Pt(msbpy)(bipz)] (**2**), [Pt(tbbpy)(mepz)] (**3**) and [Pt(msbpy)(mepz)] (**4**), where tbbpy and msbpy represent 4,4'-di-t-butyl-2,2'-bipyridine and 4,4'-dimesityl-2,2'-bipyridine, respectively. Single crystal X-ray structural analyses on **2** and **3** were executed to unveil the basic coordination geometry around the Pt(II) center as well as the π-π stacking interaction in solid state. These complexes are essentially non-emissive in solution (Q. Y. = 0.2 ~ 0.4%), but are highly luminescent in solid state with Q. Y. of 52% and 83% and τ_{obs} of 368 ns and 8.37 μs for **1** and **3**, respectively. Their photophysical properties were measured and discussed under the basis of computational approaches. For application, non-doped organic light emitting diodes (OLEDs) were fabricated using **1** and **3** as emitter, exhibiting red-orange emission with maximum luminance of 43000 cd·m^{-2}, EQE of 19.0 %, CE of 21.0 cd·A^{-1} and PE of 15.5 lm·W^{-1}, and yellow emission with maximum luminance of 5100 cd·m^{-2}, EQE of 7.1 %, CE of 21.0 cd·A^{-1} and PE of 11.3 lm·W^{-1}, respectively. The particularly higher OLED efficiencies of **1** versus **3** highlight the design principle of Pt(II) based phosphors, particularly for fabrication of non-doped OLED architecture.

_____

Introduction

Transition-metal based light-emitting materials have been receiving considerable attention owing to their potential in fabrication of the highly efficient organic light emitting diodes (OLEDs) and other optoelectronic devices.[1-10] During the past two

decades, much endeavor has been devoted to designing such phosphors with various emission hues and functionalities. Chromophoric chelates bearing single pyridyl group and anionic pendent such as functional cyclometalate and azolate have been extensively applied to build up the robust coordination frameworks for which the associated electronic properties can be fine-tuned.[11, 12] Representative examples include the Ir(III) metal complexes such as [Ir(piq)$_2$(acac)],[13] [Ir(ppy)$_2$(acac)] (acac = acetylacetonate)[14] and [Ir(dfppy)$_2$(pytz)] (piqH: 2-phenylisoquinoline, ppyH: 2-phenylpyridine, dfppyH: 2,4-difluorophenylpyridine and pytzH: 3-trifluromethyl-5-(2-pyridyl)-1,2,4-triazole),[15] among which all chelates are monoanionic and the resulting metal complexes are brightly emissive in both fluid and solid states, allowing the fabrication of efficient OLEDs that showed the anticipated RGB chromaticity.

The second class of chelates is ascribed to those with no net anionic charge, e.g., diolefin,[16] diimine,[17-21] bis-carbene[22-24] or diphosphine,[25, 26] which are equally useful in making luminescent metal complexes with versatile structural designs and diverse electronic properties. In yet another approach, from the viewpoint of formal charge residing on the chelate, metal complexes assembled with dianionic bidentate chelates should be of equal importance. The incorporation of dianion chelates is believed to alter the properties of metal complexes per se (cf. those with mono-anionic or neutral chelates), particularly from the practical concerns of stability and/or spectral tunability.

diolefin   diimine   bis-carbene   diphosphine
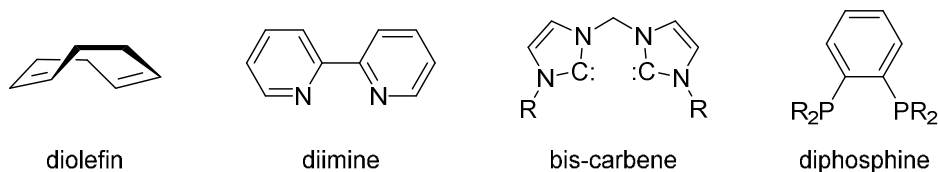
However, reports regarding dianion chelated metal complexes are sparse. Documented precedence may be ascribed to the dianionic 2,2'-biphenyl, which is capable of affording well characterized Ir(III) and Pt(II) metal phosphors,[27, 28] while dianionic chelates were utilized in synthesis of specialized Pt(II) and Pd(II)

phosphors.[29-31] As another example, 2,2'–biimidazole might have potential to serve as the dianionic chelate; unfortunately, due to the lack of electron withdrawing groups, it tends to retain both of its protons[32, 33] or only affords partial deprotonation after coordination to the transition metal.[33]

biphenyl   diimidazole   bipzH$_2$ mepzH$_2$
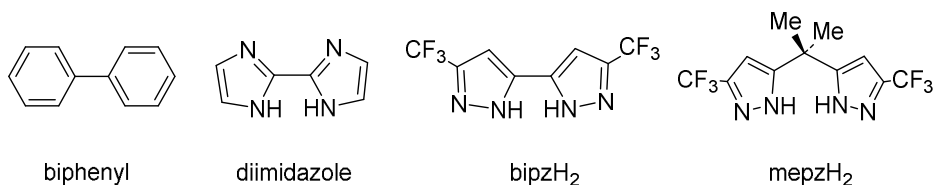
In the present work, our aims are focused on the preparation of stable luminescent metal complexes with potentially dianionic chelates such as bipyrazole with dual CF$_3$ substituents,[34, 35] e.g. bipzH$_2$ and mepzH$_2$. We also expect these metal complexes would reveal distinctive photophysical properties compared with the traditional metal phosphors with monoanionic chelates, particularly in the fabrication of non-doped organic light emitting diodes (OLEDs). Detail of results and discussion are elaborated in the following sections.

Experimental section:

General Procedures. All reactions were performed under nitrogen. Solvents were distilled from appropriate drying agents prior to use. Commercially available reagents were used without further purification. The 4,4'-dimesityl-2,2'-bipyridine (msbpy) was synthesized according to procedures in literature.[36] All reactions were monitored by TLC with pre-coated silica gel plates (Merck, 0.20 mm with fluorescent indicator UV254). Flash column chromatography was carried out using silica gel obtained from Merck (230-400 mesh). Mass spectra were obtained on a JEOL SX-102A instrument operating in electron impact (EI) or fast atom bombardment (FAB) mode. ^{1}H and ^{19}F NMR spectra were recorded on a Bruker-400 or INOVA-500 instrument. Elemental analysis was carried out with a Heraeus CHN-O Rapid Elementary Analyzer.

Synthesis of bipzH₂: To a dried THF (50 mL) solution of sodium methoxide (0.69 g, 12.79 mmol) were added ethyl trifluoroacetate (1.82 g, 12.82 mmol) and 2,3-butanedione (0.50 g, 5.81 mmol) at 0 °C under nitrogen atmosphere. The resulting mixture was stirred at RT for 24 h under N_2. The solvent was stripped off, while the residue was taken into excess ethyl acetate. The solution was then neutralized with dilute HCl solution to pH ~ 4, washed with water three times, dried over $MgSO_4$ and concentrated by rotary evaporation. The obtained solid was next treated with hydrazine monohydrate (1.4 mL, 29.12 mmol) in refluxing ethanol for 24 h. Flash column chromatography (ethyl acetate : hexane = 1 : 1) gave the product (0.43 g, 1.59 mmol, 27 %).

Selected spectral data of bipzH₂. MS (EI), observed (actual): m/z 270 (270) [M]⁺. ¹H NMR (400 MHz, acetone-d_6, 298K): δ 13.53 (s, 2H), 7.16 (s, 2H). ¹⁹F (470 MHz, CDCl₃, 294 K): δ -62.74 (s, CF₃). Anal. Calcd. for $C_8H_4F_6N_4$: C, 35.57; N, 20.74; H, 1.49. Found: C, 35.29; N, 20.93; H, 1.27.

Synthesis of mepzH₂: To a THF (50 mL) suspension of sodium methoxide (0.53 g, 9.8 mmol) were added ethyl trifluoroacetate (1.22 g, 8.59 mmol) and 3,3-dimethyl-2,4-pentanedione (0.50 g, 3.91 mmol) at 0 °C under nitrogen. The resulting mixture was stirred at RT for 24 h under N_2 and stripped to dryness under vacuum. The residue was taken into the excess of ethyl acetate. The solution was washed with dilute HCl solution and deionized water, dried over $MgSO_4$ and concentrated by rotary evaporation. Finally the crude product was treated with hydrazine monohydrate (0.5 mL, 9.70 mmol) in refluxing ethanol for 24 h. Flash column chromatography (ethyl acetate : hexane = 1 : 1) afford mepzH₂ (0.22 g, 0.70 mmol, 18 %).

Selected spectral data of mepzH₂. MS (EI), observed (actual): m/z 312 (312) [M]⁺. ¹H NMR (400 MHz, acetone-d_6, 298K): δ 12.71 (s, 2H), 6.55 (s, 2H), 1.86 (s, 6H). ¹⁹F NMR (470 MHz, acetone-d_6, 294 K): δ -62.48 (s, CF₃). Anal. Calcd. for $C_{11}H_{10}F_6N_4$: C,

42.32; N, 17.94; H, 3.23. Found: C, 42.38; N, 17.62; H, 3.75.

Synthesis of [Pt(tbbpy)(bipz)] (1): A mixture of $Pt(DMSO)_2Cl_2$ (600 mg, 1.5 mmol) and tbbpy (429 mg, 1.6 mmol) in 20 mL of 2-methoxyethanol was refluxed for 3 h to afford the intermediate complex $Pt(tbbpy)Cl_2$. Without further purification, to this reaction mixture were added $bipzH_2$ (500 mg, 1.6 mmol) and NaOAc (396 mg, 4.8 mmol), and then refluxed for 4 h. After cooling back to RT, the precipitate was filtered, washed with water, ethanol and diethyl ether to afford an orange product, which was purified by vacuum sublimation at 300 °C. Yield: 71 %.

Selected spectral data of **1**. MS (FAB. ^{195}Pt), observed (actual): m/z 732 (731) $[M+1]^+$. ^{1}H NMR (400 MHz, $CDCl_3$, 294 K): δ 10.47 (d, J_{HH} = 6 Hz, 2H), 7.73 (s, 2H), 7.46 (d, J_{HH} = 6 Hz, 2H), 6.34 (s, 2H), 1.46 (s, 18H). ^{19}F NMR (470 MHz, $CDCl_3$, 294 K): δ -60.6 (s, CF_3). Anal. Calcd. for $C_{26}H_{26}F_6N_6Pt$: C, 42.68; N, 11.49; H, 3.58. Found: C, 42.87; N, 11.28; H, 3.41.

Synthesis of [Pt(msbpy)(bipz)] (2). Using the procedure described for **1**, the reaction of $Pt(DMSO)_2Cl_2$, msbpy and $bipzH_2$ in 2-methoxyethanol afforded the Pt(II) product [Pt(msbpy)(bipz)], which was sublimed at 300 °C to afford an orange solid. Yield: 73 %.

Selected spectral data of **2**. MS (FAB. ^{195}Pt), observed (actual): m/z 856 (855) $[M+1]^+$. ^{1}H NMR (400 MHz, $CDCl_3$, 294 K): δ 11.13 (d, J_{HH} = 6 Hz, 2H), 7.77 (s, 2H), 7.59 (d, J_{HH} = 6 Hz, 2H), 6.98 (s, 4H), 6.59 (s, 2H), 2.33 (s, 6H), 2.06 (s, 12H). ^{19}F NMR (470 MHz, $CDCl_3$, 294 K): δ -60.7 (s, CF_3). Anal. Calcd. for $C_{36}H_{30}F_6N_6Pt$: C, 50.53; N, 9.82; H, 3.53. Found: C, 50.19; N, 9.73; H, 3.77.

Selected crystal data of **2**: $C_{36}H_{30}F_6N_6Pt$; M = 1025.60; T = 150(2) K; λ(Mo-K$_\alpha$) = 0.71073 Å; monoclinic; space group = $P2_1/n$; a = 11.3477(11), b = 17.9505(16), c = 19.3631(18) Å, β = 95.698(2)°; V = 3924.7(6) Å^3; Z = 4; ρ_{calcd} = 1.736 g·cm^{-3}; μ = 3.913 mm^{-1}; $F(000)$ = 2016; crystal size = 0.37 × 0.25 × 0.20 mm^3; 27188 reflections collected, 8997 independent reflections (R_{int} = 0.0462), max. and min. transmission = 0.5083 and 0.3254, restraints / parameters = 0 / 502, GOF = 1.045, final $R_1[I > 2\sigma(I)]$ =

0.0444 and wR$_2$(all data) = 0.1268, largest diff. peak and hole = 1.459 and -1.876 e·Å^{-3}.

Synthesis of [Pt(tbbpy)(mepz)] (3). Using the procedure described for **1**, the reaction of Pt(DMSO)$_2$Cl$_2$, tbbpy and mepzH$_2$ afforded the Pt(II) product complex [Pt(tbbpy)(mepz)], which was sublimed at 300 °C to afford a light yellow solid. Yield: 62 %.

Selected spectral data of **3**. MS (FAB. ^{195}Pt), observed (actual): m/z 774 (773) [M+1]$^+$. ^{1}H NMR (400 MHz, CDCl$_3$, 294 K): δ 9.80 (d, J_{HH} = 6 Hz, 2H), 8.00 (s, 2H), 7.28 (d, J_{HH} = 6 Hz, 2H), 6.27 (s, 2H), 1.74 (s, 6H), 1.16 (s, 18H). ^{19}F NMR (470 MHz, CDCl$_3$, 294 K): δ -60.2 (s, CF$_3$). Anal. Calcd. for C$_{29}$H$_{32}$F$_6$N$_6$Pt: C, 45.02; N, 10.86; H, 4.17. Found: C, 44.72; N, 10.79; H, 4.33.

Selected crystal data of **3**: C$_{29}$H$_{32}$F$_6$N$_6$Pt; M = 858.62; T = 150(2) K; λ(Mo-K$_\alpha$) = 0.71073 Å; orthorhombic; space group = *Pbcn*; a = 14.7879(6), b = 18.8945(7), c = 23.5291(10) Å; V = 6574.3(5) Å^3; Z = 8; ρ$_{calcd}$ = 1.735 g·cm^{-3}; μ = 4.496 mm^{-1}; F(000) = 3376; crystal size = 0.20 × 0.20 × 0.15 mm^3; 48712 reflections collected, 7558 independent reflections (R$_{int}$ = 0.0675), max. and min. transmission = 0.5520 and 0.4667, restraints / parameters = 10 / 425, GOF = 1.043, final R$_1$[I > 2σ(I)] = 0.0370 and wR$_2$(all data) = 0.0879, largest diff. peak and hole = 1.354 and -1.058 e·Å^{-3}.

Synthesis of [Pt(msbpy)(mepz)] (4). Using the procedure described for **1**, the reaction of K$_2$PtCl$_4$, msbpy and mepzH$_2$ afforded the Pt(II) complex [Pt(msbpy)(mepz)], which was sublimed at 300 °C to afford a yellow solid. Yield: 52 %.

Selected spectral data of **4**. MS (FAB. ^{195}Pt), observed (actual): m/z 898 (897) [M+1]$^+$. ^{1}H NMR (400 MHz, CDCl$_3$, 294 K): δ 10.28 (d, J_{HH} = 6 Hz, 2H), 7.78 (s, 2H), 7.50 (d, J_{HH} = 6 Hz, 2H), 6.96 (s, 4H), 6.40 (s, 2H), 2.32 (s, 6H), 2.04 (s, 12H), 1.95 (s, 6H). ^{19}F NMR (470 MHz, CDCl$_3$, 294 K): δ -60.4 (s, CF$_3$). Anal. Calcd. for C$_{39}$H$_{36}$F$_6$N$_6$Pt·H$_2$O: C, 51.15; N, 9.18; H, 4.18. Found: C, 51.32; N, 9.34; H, 4.64.

X-ray Structural Analysis. All single-crystal X-ray diffraction data were measured on a Bruker Smart CCD diffractometer using λ(Mo-K$_\alpha$) radiation (λ = 0.71073 Å). The data collection was executed using the SMART program. Cell refinement and data reduction were made with the SAINT program. The structure was determined using the SHELXTL/PC program and refined using full matrix least-squares. All non-hydrogen atoms were refined anisotropically, whereas hydrogen atoms were placed at the calculated positions and included in the final stage of refinements with fixed parameters. CCDC-1413686 and 1413687 contain the supplementary crystallographic data for this paper. These data can be obtained free of charge from the Cambridge Crystallographic Data Centre via http://www.ccdc.cam.ac.uk.

Spectroscopic and Dynamic Measurements. Steady-state absorption and emission spectra were recorded with a Hitachi (U-3900) spectrophotometer and an Edinburgh Fluorescence spectrometer (FLS920-t module), respectively. Both wavelength-dependent excitation and emission response of the fluorimeter have been calibrated. A configuration of front-face excitation was used to measure the emission of the solid sample, in which the cell was made by assembling two edge-polished quartz plates with various Teflon spacers. A combination of appropriate filters was used to avoid interference from the scattering light. To determine the phosphorescence quantum yield in solution. Coumarin 480 (λ$_{max}$ = 473 nm, Q.Y. = 0.87 in methanol) was used as the standard. To obtain the PL quantum yield in solid state, the emission was collected via an integrating sphere, and the quantum yield was calculated according to a reported method.[37] For lifetime measurement, data were fitted by the sum of exponential functions with a temporal resolution of ~300 ps by using a nonlinear least-squares procedure in combination with an iterative convolution method.

DFT Methodology: The molecular structures of monomers were optimized in vacuum, using the software Avogadro[38] to enter the starting geometry. The

molecular structures of dimers were optimized starting from the crystal structures with the Pt-Pt distance fixed. Then the structures were optimized, in CH_2Cl_2, starting from the optimized structure from vacuum. All calculations were carried out using the Gaussian 09 program[39] with the hybrid B3LYP functional level[40] of theory together with 6-31+G* basis set for C, H, N and F atoms and LANL2DZ basis set for Pt. Time-dependent DFT calculations (TD-DFT) were performed using Gaussian 09 program with a polarizable continuum model (PCM) in CH_2Cl_2.[41] The 70 lowest singlet electronic transitions were calculated and processed with the GaussSum software package.[42]

OLED Fabrication and Measurement. All devices were fabricated on commercial ITO-coated glass substrates. The ITO substrates were treated in order by ultrasonic bath sonication of detergent, de-ionized water, isopropanol and acetone, each with a 20 min interval. Then the ITO substrates were dried with nitrogen gas and baked in an oven at 80°C for 30 min. Subsequently, the substrates were transferred into a thermal evaporator, where the organic, inorganic and metal functional layers were grown layer by layer at a base pressure better than 4×10^{-4} Pa. The evaporation rates were monitored with several quartz crystal microbalances located above the crucibles and thermal boats. For organic semiconductors and metal oxides, the typical evaporation rates were about 0.1 nm/s and for aluminum, the evaporation rate was about 1 to 5 nm/s. The intersection of Al and ITO forms a 1 mm × 1 mm active device area. Current density-voltage (J-V) and luminance-voltage (L-V) data were collected with a source meter (Yokogawa GS610) and a luminance meter (Konica Minolta LS-110) with a customized Labview program. The electroluminance spectra were measured with a spectrophotometer (Photo Research Inc., PR-705).

Results and Discussion

Preparation and Characterization The demanded 3,3'-bipyrazole chelates, i.e. 5,5'-di(trifluoromethyl)-3,3'-bipyrazole (bipzH$_2$) and 5,5'-(1-methylethylidene)-bis

(3-trifluoromethyl-1H-pyrazole) (mepzH$_2$), were obtained from a two-step protocol, i.e. Claisen condensation employing ethyl trifluoroacetate and 2,3-butanedione and from ethyl trifluoroacetate and 3,3-dimethylpentane-2,4-dione, followed by hydrazine cyclization in refluxing ethanol. Recrystallization and sublimation were used for purification of these products. ^{1}H NMR analysis of bipzH$_2$ gives two equal intensity peaks at δ 13.53 and 7.16 in d$_6$-acetone, which are assigned to the pyrazolic NH and CH signals, respectively. In contrast, the corresponding ^{1}H NMR signals of the pyrazolic NH and CH signals for mepzH$_2$ appeared at δ 12.71 and 6.55 in d$_6$-acetone. In this case, the high-field shifting of both signals is due to the electron donating effect of the bridging methylethylidene, for which the respective methyl signal is located at δ 1.86.

The preparation of Pt(II) complexes were next accomplished in a two-step sequence. Firstly, the 2,2'-bipyridine chelate (i.e. tbbpy or msbpy) was reacted with Pt(DMSO)$_2$Cl$_2$ to afford the bipyridine intermediate, e.g. Pt(tbbpy)Cl$_2$ and Pt(msbpy)Cl$_2$. The intermediate obtained was then reacted with the bipyrazole chelate (bipzH$_2$ or mepzH$_2$) in the presence of NaOAc to afford the desired products, i.e. [Pt(tbbpy)(bipz)] (**1**), [Pt(msbpy)(bipz)] (**2**), [Pt(tbbpy)(mepz)] (**3**) and [Pt(msbpy)(mepz)] (**4**). The products were typically purified by column chromatography and recrystallization. The reaction yields run up to 73%. It is notable that all bipyridine chelates deliberately incorporated the functional substituents *t*-butyl or mesityl group at the 4,4'-position, the purpose is to improve the solubility of the Pt(II) complexes in the solution phase. The sample purities were verified by mass, ^{1}H and ^{19}F NMR and elemental analyses. Their structural drawings are depicted in Scheme 1. Notable inter-ligand H-bonding interaction between bipyridine and bipz chelates is observed for the Pt(II) complexes **1** and **2**,[43] which is confirmed by the downfield ^{1}H NMR signal observed at δ 10.49 and 11.13 versus the ^{1}H NMR signal at δ 9.80 and 10.28 of the mepz-containing Pt(II) complexes **3** and **4**, respectively. It is believed that the puckered arrangement of the mepz chelate would forfeit formation

of such H-bonding around the coordination sphere of the Pt(II) metal atom.
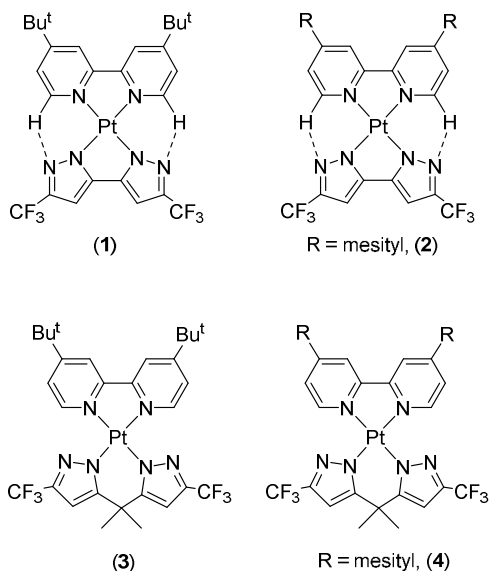
Scheme 1. Schematic drawings of the Pt(II) complexes **1** ~ **4**.

The X-ray structural analysis of **2** was conducted to show the generalized structural arrangement and packing behavior of bipz substituted Pt(II) complexes in the solid state. Figure 1 shows the ORTEP diagram of **2**, along with a simplified packing diagram showing the π-π stacking interactions between molecules in close contact. The Pt-N(pyrazolate) bond lengths of **2** are observed to be 2.001(5) and 2.009(5) Å, which are slightly longer than the Pt-N(pyrazolate) distances of 1.98 Å observed in the closely related Pt(II) complexes, but are statistically identical to those of the Pt-N(pyridine) distances of 2.019(5) Å within the same molecule. These metric data imply the possession of similar Pt-N bond strength between all nitrogen donors, despite the negative charges of the pyrazolates which should interact more strongly with the positively charged Pt(II) metal versus the neutral pyridine fragments. The double five-membered ring structure of the bis-pyrazolate chelate may induce an unfavorable strain energy at the C-C linkage between the pyrazolate fragments upon coordination, which would slightly weaken the metal-chelate bonding. Apparently, this coordination arrangement also affects the inter-ligand

bonding interaction between the msbpy and bipz chelates, for which the observed C-H⋯N distances of ~2.316 Å are also longer than the typical non-bonding distances of 2.256 ~ 2.296 Å observed in the relevant Pt(II) complexes.[44]

Substantial intermolecular interactions were also observed in the crystal lattice, which is shown by an anti-parallel stacking, with the bipz chelate of one molecule residing on top of the bpy chelate of the adjacent molecule and vice versa. A short Pt⋯Pt separation of 3.454 Å was calculated between each half of the dimer, which is comparable to the typical Pt-Pt contacts observed in several dimeric structures of cyclometalated Pt(II) complexes (3.15-3.76 Å), confirming the co-existence of π-π stacking interaction.[45-48] Furthermore, the coordination framework around each Pt(II) atom is bent outward, while the mesityl substituents on bipyridine are twisted accordingly to make more room for the CF_3 substituents of the bipz chelates of adjacent molecule.

The single crystal X-ray analysis of mepz substituted Pt(II) complex **3** was also conducted to reveal the difference with that of the bipz-containing complexes **1** and **2**. The ORTEP diagram and metric parameters are depicted in Figure 2. As can be seen, all Pt-N distances are more-or-less identical with each other as expected, except that the N-Pt-N bite angle of the mepz chelate (84.55°) is slightly greater than that of the corresponding tbpy chelate (79.49°), or that of the bipz chelate in **2** (78.3°), due to the puckered arrangement of the mepz chelate. This coordination configuration is also consistent with the ^{1}H NMR spectral data, showing absence of the inter-ligand C-H⋯N bonding interaction. Furthermore, the pair of closest molecules in the crystal lattice now adopt a nearly 90° rotated conformation, rather than the parallel alignment as observed in **2**. Most importantly, the elongated Pt⋯Pt contact of 4.505 Å eliminates the possibility for substantial intermolecular Pt⋯Pt stacking interaction.

Photophysical Characterization. The UV-Vis absorption spectra of all Pt(II) complexes in CH_2Cl_2 solution are shown in Figure 3, while pertinent data are listed in

Table 1. The intense short wavelength absorptions (< 330 nm) are due to the intra-ligand π-π* transitions, while the long wavelength absorptions between 330 - 420 nm could be tentatively assigned to the admixture of metal-to-ligand (bipyridine) charge transfer (MLCT) and ligand-to-ligand charge transfer transitions (LLCT), i.e. the transition from pyrazolate-metal fragment to bipyridine.[49-51] It is notable that the absorption onset of the lower energy bands follows a trend of **1** ~ **3** < **2** ~ **4** in terms of wavelength, together with an increase in absorptivity for the msbpy coordinated Pt(II) complexes **2** and **4**. This trend is consistent with both the greater electronegativity and π-conjugation of mesityl groups, which would afford the detected bathochromic shift and hyperchromic effect. Moreover, the lowest energy absorption band of **1** and **2** is coincident with that of **3** and **4**, respectively, showing the indistinguishable electronic character exerted by both bipz and mepz chelates in solution.

Moreover, these Pt(II) complexes exhibited relatively weak emission in CH_2Cl_2 solution with quantum yield (∅) in the range 0.2 ~ 0.4%. As can be seen, the bipz Pt(II) complexes **1** and **2** showed a much broadened emission band with peak maxima located at 633 and 629 nm, while the mepz substituted Pt(II) complexes **3** and **4** displayed a distinctive structured profile with the first peak maxima (E_{0-0}) located at 476 and 475 nm, respectively. Generally speaking, the red-shifted and structureless emission profile displayed by complexes **1** and **2** could be due to both the enhanced LLCT contribution in CH_2Cl_2 solution as showed by the DFT calculation (*vide infra*) and the possible existence of intermolecular π-π stacking interaction, the latter is essential for triggering the so-called metal-metal-to-ligand charge transfer (MMLCT) transition.[52-61] However, at the conc. of 10^{-5} M, their excitation spectra are essentially identical to the absorption spectra, implying the absence of stacked dimer or higher oligomers.

The existence of favorable π-π stacking interaction can be further confirmed by recording the emission spectra in PMMA polymer matrix with different doping levels.

As shown in Figure 4, complexes **3** and **4** bearing mepz chelates showed the concentration independent spectral patterns that also resemble their solution spectra. This result may be attributed to the lack of intermolecular interaction up to a concentration of 5 wt.% in PMMA matrix. In sharp contrast, Pt(II) complexes **1** and **2** showed notable aggregation at a much lowered concentration of 0.2 and 0.5 wt.%, respectively. Upon increase to 5 wt.%, the monomer emission is completely quenched for Pt(II) complex **1** and substantially suppressed for **2**. These results are consistent with the facile formation of dimer or even oligomer for the bipz Pt(II) complexes **1** and **2** in PMMA. In fact, dual phosphorescence has been also detected in solution state for the class of dinuclear and polynuclear Pt(II) complexes, for which the nature of excited state (e.g. monomeric emission or MMLCT) is controlled by the bridging ligand and, hence, the Pt···Pt spacing.[54, 62, 63]

Figure 5 shows the emission spectra of Pt(II) complexes **1** – **4** as neat powder, for which the emission quantum yields are substantially greater than those recorded in solution state at RT. In general, the higher emission efficiency is attributable to the rigid environment in the solid state, which then destabilizes the metal centered dd excited states and increases the corresponding emission efficiency.[25, 64] Moreover, the mepz coordinated complexes **3** and **4** retain a much blue-shifted emission profile versus their bipz counterparts **1** and **2**. These photophysical properties, together with the multiple vibronic bands and longer emission lifetime (τ_{obs} = 8370 and 2180 ns) observed, symbolize the possession of higher degree of the intra-ligand π-π* transition and reduced MLCT contribution in the emitting excited states.[64-69] Remarkably, both the bipz complexes **1** and **2** show a distinctive structureless emission with much red-shifted peak maxima centered at 633 and 629 nm and with significantly shorter lifetime of 368 and 370 ns, respectively. Apparently, these discrepancies are induced by the favorable Pt···Pt stacking interaction expected for the planar geometry of Pt(II) complexes, for which the X-ray structural analysis of **2** has unambiguously confirmed the formation of dimeric architecture with shortened

Pt···Pt separation of 3.484 Å. Moreover, since the *t*-butyl substituents in **1** are much smaller than the mesityl substituents in **2**, it is possible that the Pt(II) complex **1** should be more susceptible to form the aggregated dimer or even higher nuclearity oligomer in the solid state. Hence, the stronger intermolecular stacking interaction expected for both Pt(II) complexes **1** and **2** would result in a higher degree of red-shifting in emission versus that of the mepz substituted complexes **3** and **4**. In fact, the spectroscopic characteristics of complexes **1** and **2** are consistent with the aforementioned MMLCT excited state character that is detected in many strongly aggregated Pt(II) metal complexes.[52-60]

Theoretical Calculations. All calculations were carried out using the hybrid B3LYP functional level of theory together with 6-31+G* basis set for C, H, N and F atoms and LANL2DZ basis set for Pt. This has proven to be successful with Pt complexes without a long-range separated charge-transfer system.[70]

The contributions from component parts of the molecules to selected molecular orbitals are shown in Table S1 with numerical values detailed in Tables S3 - 6. Table S2 gives the corresponding orbital energies. For all four complexes, the LUMO and LUMO+1 are more than 93% located on the bpy ligand. For **1** and **2**, the HOMO is more than 90% located on the bipz with the HOMO-1 and HOMO-2 distributed on the Pt metal and bipz. For **3** and **4**, the HOMO shows a lower contribution of about 70% from the mepz with 30% on Pt. The HOMO-1 is distributed on the Pt metal and mepz while the HOMO-2 is mainly on the mepz. When replacing bipz with mepz, the HOMO energy decreased while the LUMO remained the same due to the location of the LUMO on the bipyridine component for all complexes.

Time-dependent DFT (TD-DFT) calculations were also performed and the simulated absorption spectra matched well with the experimental spectra. The 70 lowest-energy singlet-singlet transitions are summarized in Tables S7-10 and a representation of the low-energy excited states and transitions is shown in Figure 6. The first two electronic transitions from HOMO → LUMO and HOMO-1 → LUMO,

respectively, for **1** and **2**, both have very low oscillator strength (less than 0.01) and correspond to the tail in the experimental spectra. The first strong band (oscillator strength > 0.2), which is the third excited state, is mainly due to HOMO-2 $\rightarrow$ LUMO, with mixed MLCT and LLCT character. For **3** and **4**, the first electronic transition from HOMO $\rightarrow$ LUMO is also very weak. The second, more intense, transition is mainly due to HOMO-1 $\rightarrow$ LUMO, with some contribution from HOMO-3 $\rightarrow$ LUMO, and again possesses mixed MLCT and LLCT character. Qualitatively, we can see a similarity between HOMO-2 for **1,2** and HOMO-1 for **3,4** (Figure 6), consistent with the different character of the lowest strong transition for **1,2** and **3,4**, respectively.

Triplet excited states, which are generally lower in energy, are very important in the heavy transition metal complexes, due to spin-orbit coupling introduced by the central heavy metal which favors the formation of low-lying triplet excited states. Thus, the lowest triplet excited state was also optimized and the estimated emission energy determined by subtracting the total energy of the S_0 state from that of the minimized T_1 state, both at the minimized T_1 state geometry. The results are summarized in Table S11 and shown pictorially on Figure 6. These calculations predict a lower-energy emission for **1,2** compared with **3,4**, and this can be correlated with the lower-energy HOMO for **3** and **4** that also leads to a lower S_1. This suggests that the solution red-shift of emission for **1** and **2** compared with **3** and **4** is largely intrinsic to the molecules, rather than being attributable to aggregation. The aggregation then leads to a further red-shift in keeping with the experimental results shown in Figure 5.

To probe the role of aggregation, we carried out calculations on dimers of **1** with the Pt-Pt distance fixed at 3.484 Å or 3.44 Å during optimization (Table S12). This showed a lowering of energy as the Pt-Pt distance was shortened of -0.19 eV and -0.24 eV per complex respectively compared with the isolated monomer. This stabilization is consistent with the aggregation in solution and solid state observed during the photophysical studies.

Non-doped OLED Performance of 1 and 3. The high quantum efficiency of **1** and **3** in neat film encouraged us to fabricate the corresponding electrophosphorescent devices. A non-doped structure of ITO/MoO$_3$ (2 nm)/ 1,4-bis(1-naphthylphenylamino)-biphenyl (NPB) (25 nm)/ 1,3-bis(9-carbazolyl)benzene (mCP) (8 nm)/ **1** or **3** (40 nm)/ tris[3-(3-pyridyl)mesityl]borane (3TPYMB) (50 nm)/LiF (1 nm)/Al was used, where NPB was used as the hole-transporting material; mCP was employed to facilitate hole into the emitting layer; 3TPYMB was utilized as electron-transporting material; MoO$_3$ and LiF served as hole- and electron-injecting materials, respectively . The current density-voltage-luminance (*J-V-L*) characteristics, current efficiency/power efficiency/EQE versus current density and EL spectra of the devices were shown in Figure 7. As shown in Figure 7a, the turn-on voltages (at 1 cd·m^{-2}) for **1** and **3** are 4.1 V and 5.1 V, respectively, which can be ascribed to the difference between the conductivities of **1** and **3** as can be seen from the large difference in the current densities of **1** and **3**. Maximum luminance levels for **1** and **3** were about 43000 cd·m^{-2} and 5100 cd·m^{-2}. As can be seen in Figure 7b, maximum EQE of 19.0 % and 7.1 %, maximum CE of 21.0 cd·A^{-1} and 21.0 cd·A^{-1}, and maximum PE of 15.5 lm·W^{-1} and 11.3 lm·W^{-1} were achieved for **1** and **3**, respectively. It is remarkable that the EQE for the non-doped device of **1** is already comparable or even superior to the doped results based on the red-emitting Pt(II) and Ir(III) counterparts.[71-74] Moreover, at high current density of 100 mA·cm^{-2} (12800 cd·m^{-2}, 10.6 V), the EQE value still remained as high as 12.8%, indicating the low efficiency roll-off characteristic of **1**. As a comparison, the device for **3** shows much lower efficiency and pronounced efficiency roll-off (with an EQE of 1.7 % at 100 mA·cm^{-2}). The difference between **1** and **3** is assumed to be mainly caused by the large difference between the exciton dynamics. Complex **1** shows a much shorter triplet exciton lifetime of 368 ns (as shown in Table 1), which is 20 times shorter than that of **3**. In addition to the balanced carrier transport, a shorter exciton lifetime helps to reduce the non-radiative losses, such as

triplet-triplet annihilation (TTA) and triplet-polaron annihilation (TPA), which is the key to maintain a high EQE.[75] The electroluminescence spectra of **1** and **3** are shown in Figure 7c. Slightly red shift of 7 nm were found for both **1** and **3** and the CIE 1931 coordinates for **1** and **3** are found to be (0.63, 0.37) and (0.27, 0.52), respectively.

Conclusion.

In conclusion, we have synthesized four highly emissive Pt(II) metal complexes assembled using charge-neutral bipyridine-based chelate and a dianionic heteroaromatic counterpart, such as bipz and mepz. Both the photophysical measurement and DFT calculation showed the existence of the mixed MLCT and ligand-to-ligand charge transfer (LLCT) character in their lowest energy triplet excited states, which is different from typical Pt(II) complexes with dominant MLCT and intra-ligand charge transfer (ILCT) contribution. Apparently, the dianionic chelate is the key for changing the observed electronic properties. Despite of this intrinsic difference, Pt(II) complexes **1** and **3** showed efficient emission in solid state, with Q. Y. of 52% and 83% and τ_{obs} of 368 ns and 8.37 μs, respectively. Notably, non-doped OLEDs employing the planar Pt(II) phosphor **1** exhibited red-orange emission with max. luminance of 43000 cd·m^{-2}, EQE of 19.0 %, CE of 21.0 cd·A^{-1} and PE of 15.5 lm·W^{-1}, which are much superior to the data recorded for the yellow-emitting Pt(II) reference complex **3** with a non-planar molecular geometry (c.f. max. luminance of 5100 cd·m^{-2}, EQE of 7.1 %, CE of 21.0 cd·A^{-1} and PE of 11.3 lm·W^{-1}). The high OLED efficiencies of **1** could be derived from the balanced carrier transport as well as the shortened lifetime in the sub-microsecond region. This information is of uttermost useful to a better design of transition-metal based phosphors, particularly for fabrication of non-doped OLED architecture.

Table 1. Selected photophysical properties of Pt(II) complexes **1 – 4**.

	abs $\lambda_{max}^{[a]}$ ($\varepsilon \times$ 10^{-4}, $M^{-1}cm^{-1}$)	em λ_{max} (nm)[b]	Φ (%)[b]	τ_{obs} (ns)[b]	$k_r^{[c]}$ (s^{-1})	$k_{nr}^{[c]}$ (s^{-1})
1	265 (1.79), 377 (0.57)	(580); [633]	(0.2); [52]	(22); [368]	(9.1×10^4) [1.4×10^6]	(4.5×10^7) [1.3×10^6]
2	273 (2.10), 386 (0.67)	(578); [629]	(0.4); [10]	(12); [370]	(3.3×10^5) [2.7×10^5]	(8.3×10^7) [2.4×10^6]
3	268 (1.93), 368 (0.53)	(476, 505, 540); [471, 502, 535, 581]	(0.2); [83]	(6.5); [8370]	(3.1×10^5) [9.9×10^4]	(1.5×10^8) [2.0×10^4]
4	277 (2.60), 377 (0.66)	(475, 508, 540); [484, 512, 548, 597]	(0.4); [66]	(8.7); [2180]	(4.6×10^5) [3.0×10^5]	(1.1×10^8) [1.6×10^5]

[a] UV-Vis spectra were recorded in CH_2Cl_2 solution at 1 x 10^{-5} M. [b] PL data measured in CH_2Cl_2 and in solid state as neat powder at RT are depicted in parentheses and square bracket, respectively. [c] k_r and k_{nr} were calculated according to the equations, $k_r = \Phi/\tau_{obs}$ and $k_{nr} = (1/\tau_{obs}) - k_r$.
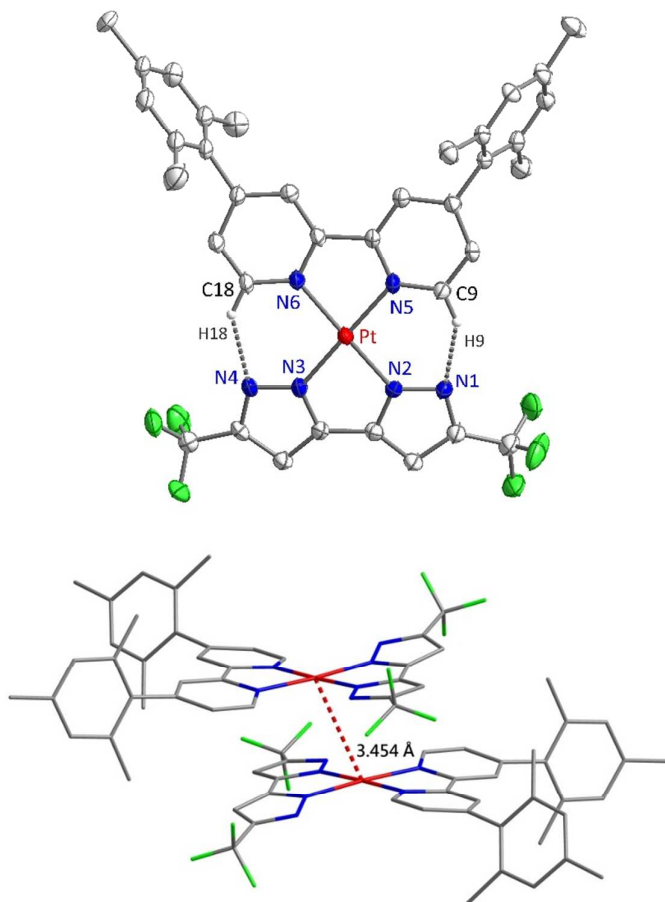
Figure 1. (top) Structural drawing of **2** with thermal ellipsoids shown at the 50% probability level. (bottom) Diagram showing the molecular stacking and closest Pt···Pt contact. Selected bond distances: Pt-N(2) = 2.001(5), Pt-N(3) = 2.009(5), Pt-N(5) = 2.019(5), Pt-N(6) = 2.019(5), N(1)···H(9) = 2.313 and N(4)···H(18) = 2.319 Å, and bond angles: N(2)-Pt-N(3) = 78.3(2) and N(5)-Pt-N(6) = 79.7(2)°.
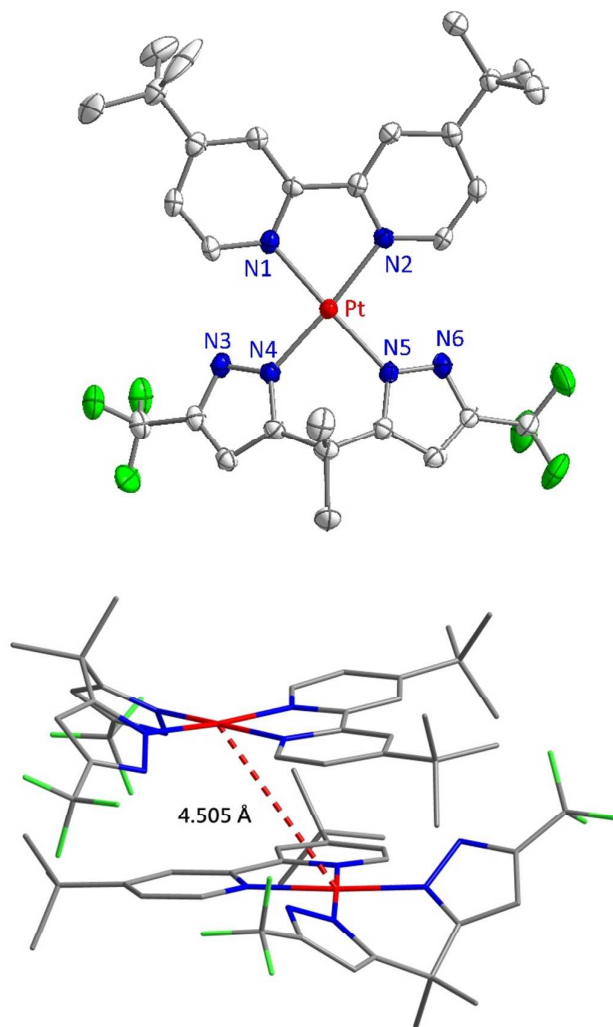
Figure 2. (top) Structural drawing of **3** with thermal ellipsoids shown at the 50% probability level. (bottom) Diagram showing the molecular stacking and closest Pt···Pt contact. Selected bond distances: Pt-N(1) = 2.021(4), Pt-N(2) = 2.025(4), Pt-N(4) = 1.994(4) and Pt-N(5) = 2.012(4) Å, and bond angles: N(1)-Pt-N(2) = 79.49(15) and N(4)-Pt-N(5) = 84.55(15)°.
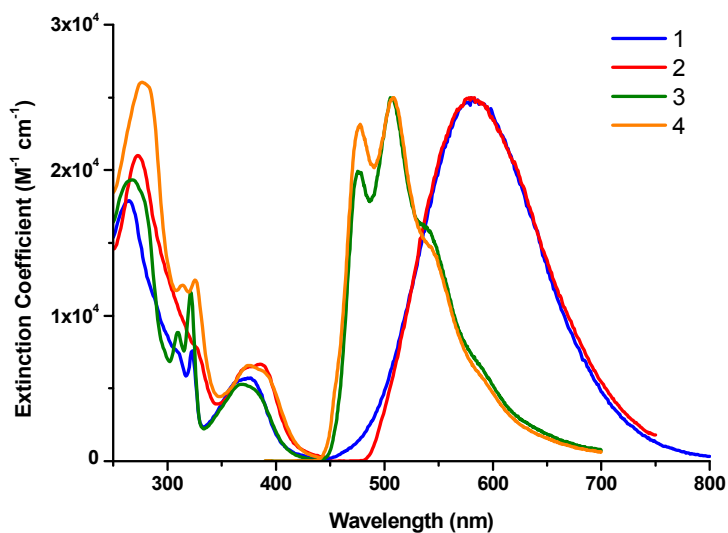
Figure 3. UV-Vis absorption and normalized emission spectra of Pt(II) complexes **1 − 4** recorded in CH₂Cl₂ solution at 1 x 10⁻⁵ M at RT.
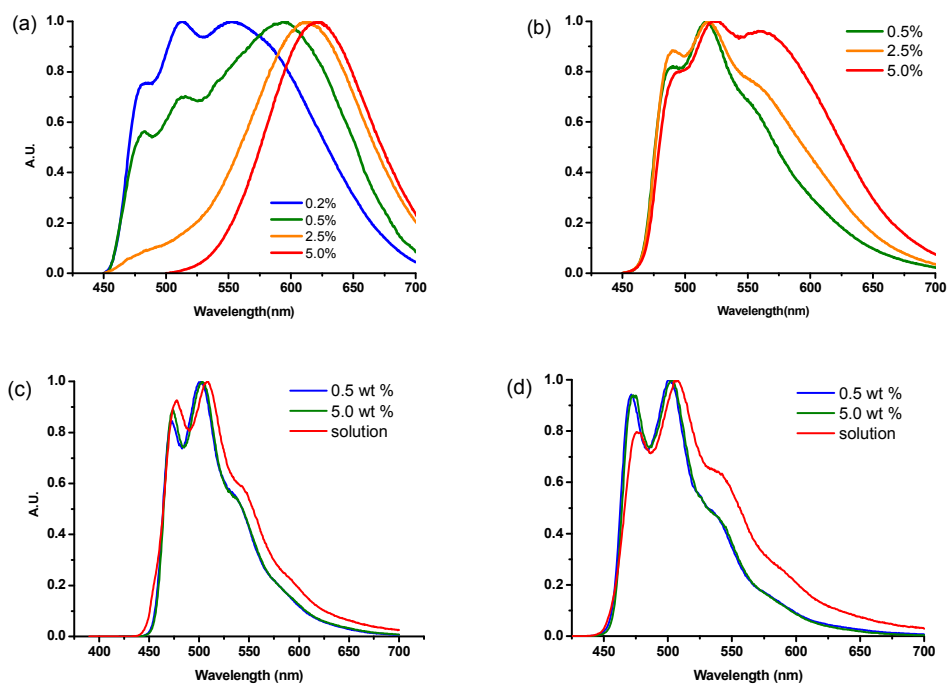

Figure 4. The normalized emission spectra of Pt(II) complexes **1 − 4** (i.e. a − d) recorded in doped PMMA thin film.
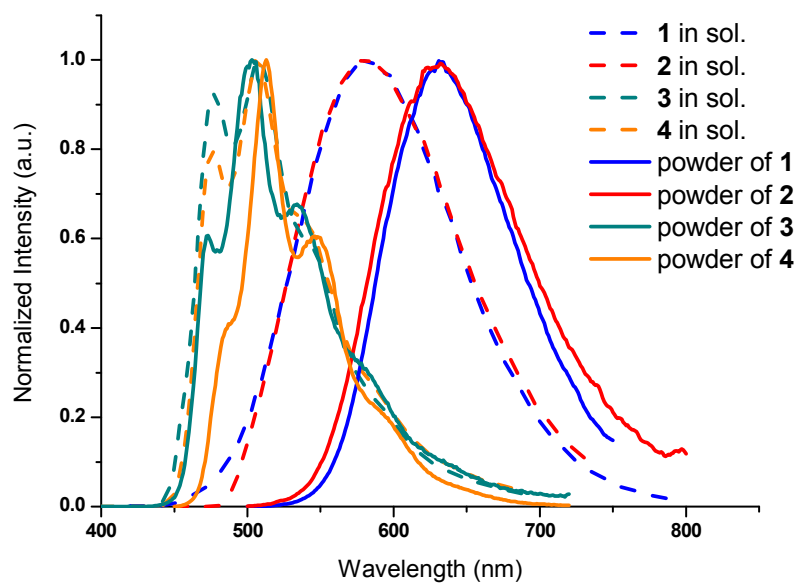
Figure 5. The normalized emission spectra of Pt(II) complexes **1** − **4** recorded in CH$_2$Cl$_2$ and as thin film of neat powder at RT.

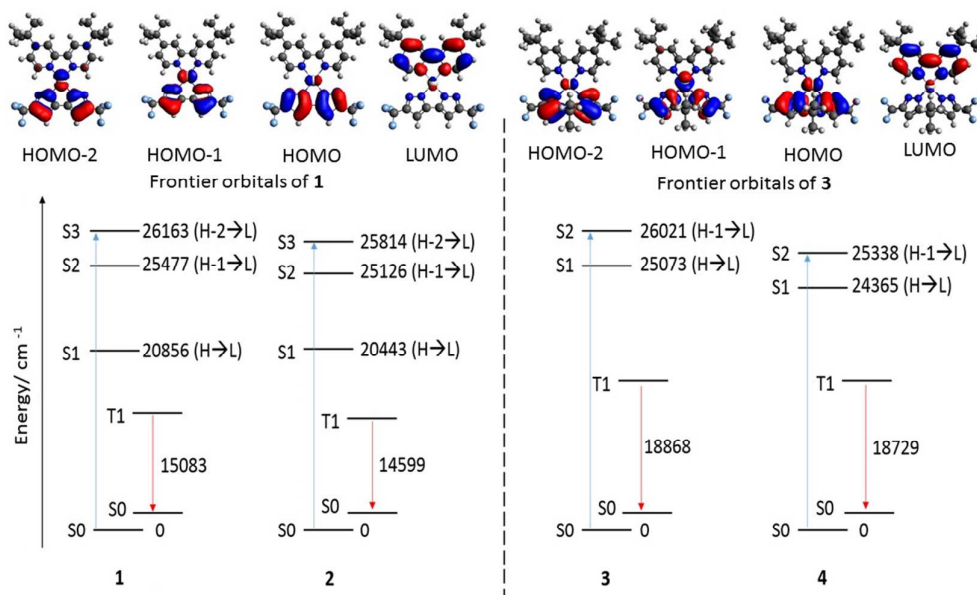**Figure 6**. Upper part: frontier orbitals involved in the lowest-lying electronic transitions illustrated for representative complexes **1** and **3**. Lower part: the lowest energy strong (oscillator strength > 0.1) transitions calculated for **1** − **4** and the calculated T_1-S_0 energy gap in the optimized T_1 geometry. Calculation were carried out with incorporation of the PCM model for CH_2Cl_2.
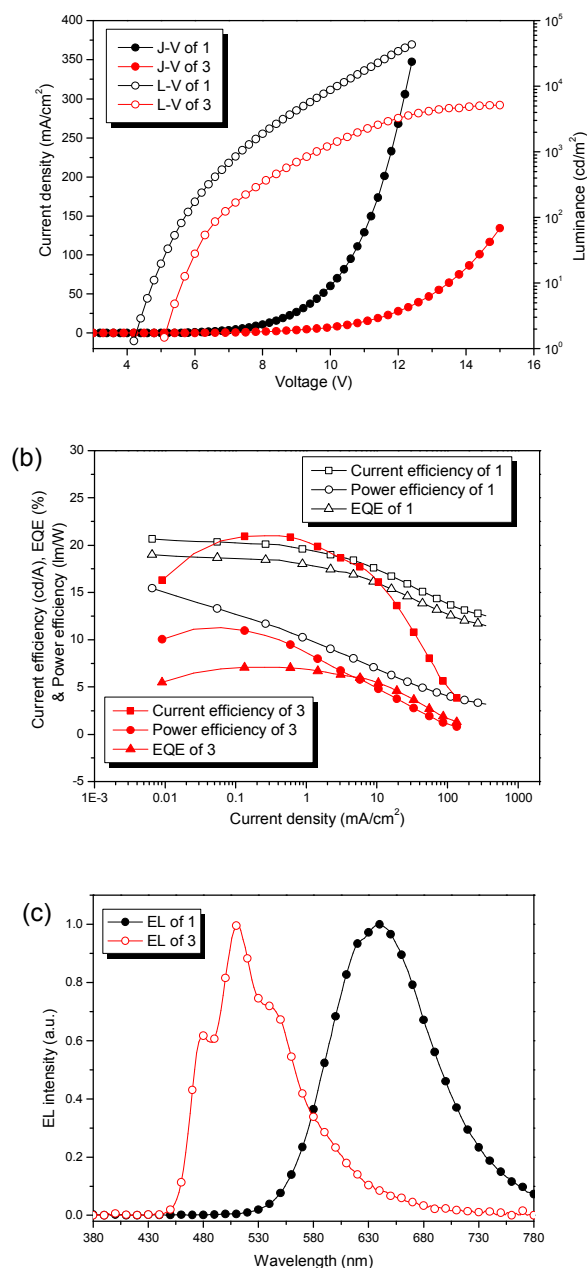
Figure 7. (a) Current density - voltage (J-V) and luminance - voltage (L-V) curves, (b) current efficiency, power efficiency and EQE curves and (c) electroluminescence spectra for non-doped devices of **1** and **3**.

References

1.   Q. Zhao, F. Li and C. Huang, *Chem. Soc. Rev.*, 2010, **39**, 3007.

2.   K. M.-C. Wong and V. W.-W. Yam, *Acc. Chem. Res.*, 2011, **44**, 424.

3.   G. Zhou, W.-Y. Wong and X. Yang, *Chem. Asian J.*, 2011, **6**, 1706.

4.   E. Baggaley, J. A. Weinstein and J. A. G. Williams, *Coord. Chem. Rev.*, 2012, **256**, 1762.

5.   Y. You and W. Nam, *Chem. Soc. Rev.*, 2012, **41**, 7061.

6.   S. Ladouceur and E. Zysman-Colman, *Eur. J. Inorg. Chem.*, 2013, **2013**, 2985.

7.   X. Zhang, Z. Chi, Y. Zhang, S. Liu and J. Xu, *J. Mater. Chem. C*, 2013, **1**, 3376.

8.   W. C. H. Choy, W. K. Chan and Y. Yuan, *Adv. Mater.*, 2014, **26**, 5368.

9.   G. Li and J. Lin, *Chem. Soc. Rev.*, 2014, **43**, 7099.

10.   X. Yang, X. Xu and G. Zhou, *J. Mater. Chem. C*, 2015, **3**, 913.

11.   Y. Chi and P.-T. Chou, *Chem. Soc. Rev.*, 2010, **39**, 638.

12.   Y. Chi, B. Tong and P.-T. Chou, *Coord. Chem. Rev.*, 2014, **281**, 1.

13.   D. Curiel, M. Mas-Montoya, C.-H. Chang, P.-Y. Chen, C.-W. Tai and A. Tarraga, *J. Mater. Chem. C*, 2013, **1**, 3421.

14.   K.-H. Kim, C.-K. Moon, J.-H. Lee, S.-Y. Kim and J.-J. Kim, *Adv. Mater.*, 2014, **26**, 3844.

15.   S.-J. Yeh, M.-F. Wu, C.-T. Chen, Y.-H. Song, Y. Chi, M.-H. Ho, S.-F. Hsu and C. H. Chen, *Adv. Mater.*, 2005, **17**, 285.

16.   C.-H. Fang, Y.-L. Chen, C.-H. Yang, Y. Chi, Y.-S. Yeh, E. Y. Li, Y.-M. Cheng, C.-J. Hsu, P.-T. Chou and C.-T. Chen, *Chem. Eur. J.*, 2007, **13**, 2686.

17.   S. Ladouceur, D. Fortin and E. Zysman-Colman, *Inorg. Chem.*, 2010, **49**, 5625.

18.   M. V. Werrett, S. Muzzioli, P. J. Wright, A. Palazzi, P. Raiteri, S. Zacchini, M. Massi and S. Stagni, *Inorg. Chem.*, 2013, **53**, 229.

19.   C.-O. Ng, S.-M. Yiu and C.-C. Ko, *Inorg. Chem.*, 2014, **53**, 3022.

20.   G. Abbott, R. Brooks, E. Rosenberg, M. Terwilliger, J. B. A. Ross and O. O. L. Ichire, *Organometallics*, 2014, **33**, 2467.

21.   R. Liu, N. Dandu, J. Chen, Y. Li, Z. Li, S. Liu, C. Wang, S. Kilina, B. Kohler and W. Sun, *J. Phys. Chem. C*, 2014, **118**, 23233.

22.   H. Uesugi, T. Tsukuda, K. Takao and T. Tsubomura, *Dalton Trans.*, 2013, **42**, 7396.

23.   T. Zou, C.-N. Lok, Y. M. E. Fung and C.-M. Che, *Chem. Commun.*, 2013, **49**, 5423.

24.   Y. Zhang, J. Clavadetscher, M. Bachmann, O. Blacque and K. Venkatesan, *Inorg. Chem.*, 2014, **53**, 756.

25.   B.-S. Du, J.-L. Liao, M.-H. Huang, C.-H. Lin, H.-W. Lin, Y. Chi, H.-A. Pan, G.-L. Fan, K.-T. Wong, G.-H. Lee and P.-T. Chou, *Adv. Funct. Mater.*, 2012, **22**, 3491.

26. J. Yuasa, M. Dan and T. Kawai, *Dalton Trans.*, 2013, **42**, 16096.

27. K. R. Lee, M.-S. Eum, C. S. Chin, S. Lee, I. J. Kim, Y. S. Kim, Y. Kim, S.-J. Kim and N. H. Hur, *Dalton Trans.*, 2009, 3650.

28. J. DePriest, G. Y. Zheng, N. Goswami, D. M. Eichhorn, C. Woods and D. P. Rillema, *Inorg. Chem.*, 2000, **39**, 1955.

29. X.-C. Hang, T. Fleetham, E. Turner, J. Brooks and J. Li, *Angew. Chem. Int. Ed.*, 2013, **52**, 6753.

30. T. Fleetham, G. Li, L. Wen and J. Li, *Adv. Mater.*, 2014, **26**, 7116.

31. Z.-Q. Zhu, T. Fleetham, E. Turner and J. Li, *Adv. Mater.*, 2015, **27**, 2533.

32. A. Savini, A. Bucci, G. Bellachioma, S. Giancola, F. Palomba, L. Rocchigiani, A. Rossi, M. Suriani, C. Zuccaccia and A. Macchioni, *J. Organomet. Chem.*, 2014, **771**, 24.

33. L. Jin, Y. Matsuda, K. Uemura and M. Ebihara, *Inorg. Chem.*, 2015, **54**, 2331.

34. H.-H. Yeh, S.-T. Ho, Y. Chi, J. N. Clifford, E. Palomares, S.-H. Liu and P.-T. Chou, *J. Mater. Chem. A*, 2013, **1**, 7681.

35. Y. Chi, K.-L. Wu and T.-C. Wei, *Chem. Asian J.*, 2015, **10**, 1098.

36. M. Chandrasekharam, G. Rajkumar, C. Srinivasa Rao, T. Suresh, M. Anil Reddy, P. Yella Reddy, Y. Soujanya, B. Takeru, Y. Jun-Ho, M. K. Nazeeruddin and M. Graetzel, *Synth. Met.*, 2011, **161**, 1098.

37. J. C. De Mello, F. H. Wittmann and R. H. Friend, *Adv. Mater.*, 1997, **9**, 230.

38. M. Hanwell, D. Curtis, D. Lonie, T. Vandermeersch, E. Zurek and G. Hutchison, *J. Cheminfor.*, 2012, **4**, 17.

39. M. J. Frisch, G. W. Trucks, H. B. Schlegel, G. E. Scuseria, M. A. Robb, J. R. Cheeseman, G. Scalmani, V. Barone, B. Mennucci, G. A. Petersson, H. Nakatsuji, M. Caricato, X. Li, H. P. Hratchian, A. F. Izmaylov, J. Bloino, G. Zheng, J. L. Sonnenberg, M. Hada, M. Ehara, K. Toyota, R. Fukuda, J. Hasegawa, M. Ishida, T. Nakajima, Y. Honda, O. Kitao, H. Nakai, T. Vreven, J. A. Montgomery, J. E. Peralta, F. Ogliaro, M. Bearpark, J. J. Heyd, E. Brothers, K. N. Kudin, V. N. Staroverov, R. Kobayashi, J. Normand, K. Raghavachari, A. Rendell, J. C. Burant, S. S. Iyengar, J. Tomasi, M. Cossi, N. Rega, J. M. Millam, M. Klene, J. E. Knox, J. B. Cross, V. Bakken, C. Adamo, J. Jaramillo, R. Gomperts, R. E. Stratmann, O. Yazyev, A. J. Austin, R. Cammi, C. Pomelli, J. W. Ochterski, R. L. Martin, K. Morokuma, V. G. Zakrzewski, G. A. Voth, P. Salvador, J. J. Dannenberg, S. Dapprich, A. D. Daniels, Farkas, J. B. Foresman, J. V. Ortiz, J. Cioslowski and D. J. Fox, *Gaussian 09, Revision D.01; Gaussian Inc.*, 2009, Wallingford, CT.

40. A. D. Becke, *J. Chem. Phys.*, 1993, **98**, 1372.

41. M. Cossi and V. Barone, *J. Chem. Phys.*, 2001, **115**, 4708.

42. N. M. O'Boyle, A. L. Tenderholt and K. M. Langner, *J. Comp. Chem.*, 2008, **29**,

839.

43.   H.-Y. Ku, B. Tong, Y. Chi, H.-C. Kao, C.-C. Yeh, C.-H. Chang and G.-H. Lee, *Dalton Trans.*, 2015, **44**, 8552.

44.   S.-Y. Chang, J. Kavitha, S.-W. Li, C.-S. Hsu, Y. Chi, Y.-S. Yeh, P.-T. Chou, G.-H. Lee, A. J. Carty, Y.-T. Tao and C.-H. Chien, *Inorg. Chem.*, 2006, **45**, 137.

45.   L. Holland, W.-Z. Shen, P. von Grebe, P. J. Sanz Miguel, F. Pichierri, A. Springer, C. A. Schalley and B. Lippert, *Dalton Trans.*, 2011, **40**, 5159.

46.   X.-H. Zhao, G.-H. Xie, Z.-D. Liu, W.-J. Li, M.-d. Yi, L.-H. Xie, C.-P. Hu, R. Zhu, Q. Zhao, Y. Zhao, J.-F. Zhao, Y. Qian and W. Huang, *Chem. Commun.*, 2012, **48**, 3854.

47.   S.-B. Ko, J.-S. Lu, Y. Kang and S. Wang, *Organometallics*, 2013, **32**, 599.

48.   H. Li, W. Yuan, X. Wang, H. Zhan, Z. Xie and Y. Cheng, *J. Mater. Chem. C*, 2015, **3**, 2744.

49.   D. P. Rillema, A. J. Cruz, C. Moore, K. Siam, A. Jehan, D. Base, T. Nguyen and W. Huang, *Inorg. Chem.*, 2013, **52**, 596.

50.   J.-L. Liao, Y. Chi, S.-H. Liu, G.-H. Lee, P.-T. Chou, H.-X. Huang, Y.-D. Su, C.-H. Chang, J.-S. Lin and M.-R. Tseng, *Inorg. Chem.*, 2014, **53**, 9366.

51.   J.-L. Liao, Y. Chi, C.-C. Yeh, H.-C. Kao, C.-H. Chang, M. A. Fox, P. J. Low and G.-H. Lee, *J. Mater. Chem. C*, 2015, **3**, 4910.

52.   V. M. Miskowski and V. H. Houlding, *Inorg. Chem.*, 1991, **30**, 4446.

53.   V. W.-W. Yam, K. M.-C. Wong and N. Zhu, *J. Am. Chem. Soc.*, 2002, **124**, 6506.

54.   W. Lu, M. C. W. Chan, N. Zhu, C.-M. Che, C. Li and Z. Hui, *J. Am. Chem. Soc.*, 2004, **126**, 7639.

55.   A. l. Díez, J. Forniés, C. Larraz, E. Lalinde, J. A. López, A. Martín, M. T. Moreno and V. Sicilia, *Inorg. Chem.*, 2010, **49**, 3239.

56.   J. S. Field, C. D. Grimmer, O. Q. Munro and B. P. Waldron, *Dalton Trans.*, 2010, **39**, 1558.

57.   Y. Nishiuchi, A. Takayama, T. Suzuki and K. Shinozaki, *Eur. J. Inorg. Chem.*, 2011, 1815.

58.   C.-T. Liao, H.-H. Chen, H.-F. Hsu, A. Poloek, H.-H. Yeh, Y. Chi, K.-W. Wang, C.-H. Lai, G.-H. Lee, C.-W. Shih and P.-T. Chou, *Chem. Eur. J.*, 2011, **17**, 546.

59.   V. Sicilia, J. Fornies, J. M. Casas, A. Martin, J. A. Lopez, C. Larraz, P. Borja, C. Ovejero, D. Tordera and H. Bolink, *Inorg. Chem.*, 2012, **51**, 3427.

60.   C. Cuerva, J. A. Campo, P. Ovejero, M. R. Torres, E. Oliveira, S. M. Santos, C. Lodeiro and M. Cano, *J. Mater. Chem. C*, 2014, **2**, 9167.

61.   A. Amar, H. Meghezzi, J. Boixel, H. Le Bozec, V. Guerchais, D. Jacquemin and A. Boucekkine, *J. Phys. Chem. A*, 2014, **118**, 6278.

62.   W. Sun, H. Zhu and P. M. Barron, *Chem. Mater.*, 2006, **18**, 2602.

63. K.-W. Wang, J.-L. Chen, Y.-M. Cheng, M.-W. Chung, C.-C. Hsieh, G.-H. Lee, P.-T. Chou, K. Chen and Y. Chi, *Inorg. Chem.*, 2010, **49**, 1372.

64. A. F. Rausch, L. Murphy, J. A. G. Williams and H. Yersin, *Inorg. Chem.*, 2012, **51**, 312.

65. Y.-L. Rao, D. Schoenmakers, Y.-L. Chang, J.-S. Lu, Z.-H. Lu, Y. Kang and S. Wang, *Chem. Eur. J.*, 2012, **18**, 11306.

66. S.-Y. Chang, J.-L. Chen, Y. Chi, Y.-M. Cheng, G.-H. Lee, C.-M. Jiang and P.-T. Chou, *Inorg. Chem.*, 2007, **46**, 11202.

67. S.-Y. Chang, J. Kavitha, J.-Y. Hung, Y. Chi, Y.-M. Cheng, E. Y. Li, P.-T. Chou, G.-H. Lee and A. J. Carty, *Inorg. Chem.*, 2007, **46**, 7064.

68. F. Nisic, A. Colombo, C. Dragonetti, D. Roberto, A. Valore, J. M. Malicka, M. Cocchi, G. R. Freeman and J. A. G. Williams, *J. Mater. Chem. C*, 2014, **2**, 1791.

69. X. Wang, S.-L. Gong, D. Song, Z.-H. Lu and S. Wang, *Adv. Funct. Mater.*, 2014, **26**, 7257.

70. W. Wu, W. Wu, S. Ji, H. Guo and J. Zhao, *Dalton Trans.*, 2011, **40**, 5953.

71. R. Meerheim, K. Walzer, M. Pfeiffer and K. Leo, *Appl. Phys. Lett.*, 2006, **89**, 061111.

72. Y. Tao, Q. Wang, C. Yang, Q. Wang, Z. Zhang, T. Zou, J. Qin and D. Ma, *Angew. Chem. Int. Ed.*, 2008, **47**, 8104.

73. C. Wu, S. Tao, M. Chen, F.-L. Wong, Y. Yuan, H.-W. Mo, W. Zhao and C.-S. Lee, *Chem. Asian J.*, 2013, **8**, 2575.

74. P.-K. Chow, G. Cheng, G. S. M. Tong, W.-P. To, W.-L. Kwong, K.-H. Low, C.-C. Kwok, C. Ma and C.-M. Che, *Angew. Chem. Int. Ed.*, 2015, **54**, 2084.

75. Q. Wang, I. W. H. Oswald, M. R. Perez, H. Jia, B. E. Gnade and M. A. Omary, *Adv. Funct. Mater.*, 2013, **23**, 5420.

TOC illustration
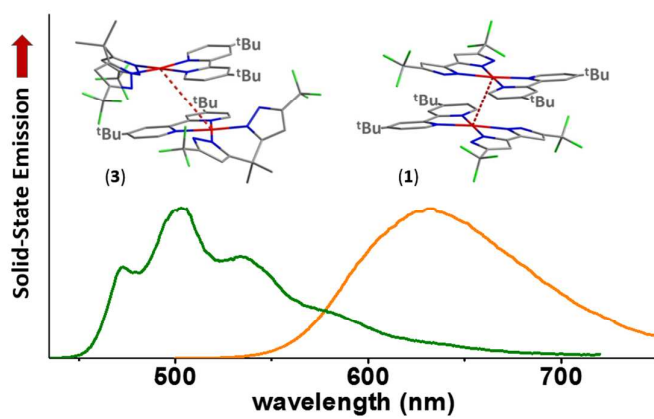
Pt(II) metal phosphor (**1**), with red-shifted emission versus non-planar counterpart (**3**), is particular suitable for fabrication of non-doped OLEDs.